Engineering Journal issn: 0125-8281

Article

Parity-Time Symmetric Capacitive Wireless Power Transfer with Extended Transfer Distance

Panavy Pookaiyaudom[a] **and Apisak Worapishet**[b,*]

Mahanakorn Institute of Innovation, Mahanakorn University of Technology, 140 Cheumsampan Rd. Nong-Chok, Bangkok 10530, Thailand
E-mail: [a]panavy@mut.ac.th, [b,*]apisak@mut.ac.th (Corresponding author)

Abstract. Despite increasing popularity of capacitive wireless power transfer as a complementary technique to its inductive counterpart, the capacitive system entails a major performance bottleneck in terms of robustness of power transfer level over separating distance due to inherently low nature of electric couplings as compared to magnetic fields. This work develops an enhanced capacitive wireless power transfer system by means of incorporating the parity-time symmetry, with the capability to maintain transferred power over a significantly extended distance. General theoretical analysis is derived for parity-time symmetric capacitive power transfer based on both series and parallel coupled resonators. A practical parity-time symmetric capacitive system with a 10-W power delivery was designed and simulated. Extensive simulation using practical components indicates more than twenty-fold increase in the transfer distance than its conventional non-parity-time-symmetric capacitive counterpart, with an efficiency over 90%.

Keywords: Wireless power transfer, capacitive coupling, parity-time symmetry.

ENGINEERING JOURNAL Volume 26 Issue 6
Received 3 May 2022
Accepted 5 June 2022
Published 30 June 2022
Online at https://engj.org/
DOI:10.4186/ej.2022.26.6.73

DOI:10.4186/ej.2022.26.6.73

1. Introduction

Over the past decade, the inductive wireless power transfer (IPT) system by means of varying magnetic fields has become ubiquitous with numerous consumer applications [1–5]. It is also anticipated to underpin many more advanced applications, including charging of in-motion electric vehicles (EV), in-flight drones, underwater vehicles etc. [3–5]. It is not until recently that the capacitive wireless power transfer (CPT) system via varying electric fields has emerged as another viable option [6–10]. The CPT embraces certain advantageous features and can be a complementary system to its IPT counterpart. In particular, the coupling plates in the CPT are lighter in weight, less expensive and simpler to implement as compared to bulky coils in the IPT system, particularly with ferrites for increased flux density. Furthermore, the CPT does not suffer from skin effects in wire coils and eddy current losses in nearby metals, which can cause high losses and high operating temperature. Another benefit includes less sensitive to coupling misalignment between transmitter (Tx) and receiver (Rx).

With increasing adoption, the CPT system is still lagging behind, particularly with regards to robustness of transferred power level against separating Tx-Rx distances due to inherently low capacitive coupling [10]. For its IPT counterpart, a technique based on parity-time ($\mathcal{PT}$) symmetry, which exhibits invariant properties under joint parity and time reversal operation [11, 12], has been incorporated and successfully demonstrated to significantly enhance power transfer robustness over the distance [13, 14]. To harness such a remarkable $\mathcal{PT}$-symmetry characteristic, it is the purpose of this letter to develop the $\mathcal{PT}$-symmetric CPT system with significantly reduced sensitivity to low and varying capacitive couplings. The $\mathcal{PT}$-symmetric CPT structure is outlined, followed by a detailed analysis and a demonstrated system with the ability to maintain delivered power level over significantly extended Tx-Rx distances than the conventional CPT. Such improvement is achieved without the need of additional active tuning circuitry, which often add considerable complexity and cost to the system.

2. Structure and Analysis

The series and parallel coupled resonator structures of the $\mathcal{PT}$-symmetric CPT ($\mathcal{PT}$-CPT) system are illustrated in Fig. 1(a) and 1(b), respectively. For each configuration, a series or parallel resonator (L_1-C_1) with a gain element (i.e., a negative resistance $-R_G$) is coupled to another series or parallel resonator (L_2-C_2) with a loss element (i.e., a positive resistance $+R_L$) by means of capacitive coupling via C_κ's. Depending on applications, the capacitor C_κ's can be implemented using two-plate, four-plate, six-plate or matrix structures [10]. Instead of employing an independent voltage/current source in the L_1-C_1 or Tx resonator, it is the incorporation of the gain element $-R_G$ that serves as the time-reversed counterpart to counterbalance the dissipation due to the loss element $+R_L$ in the L_2-C_2 or Rx resonator. Under the $\mathcal{PT}$-symmetric condition with $L_1 = L_2 = L$, $C_1 = C_2 = C$, and $-R_G + R_L = 0$ or equivalently $R_G = R_L = R$, the oscillation frequency of the injected power from the gain element (with external power P_{in}) is self-selected to balance the dissipated power at the loss element amid variation in the coupling through C_κ's, which is in turn determined by the separating distance between the capacitors' plates.

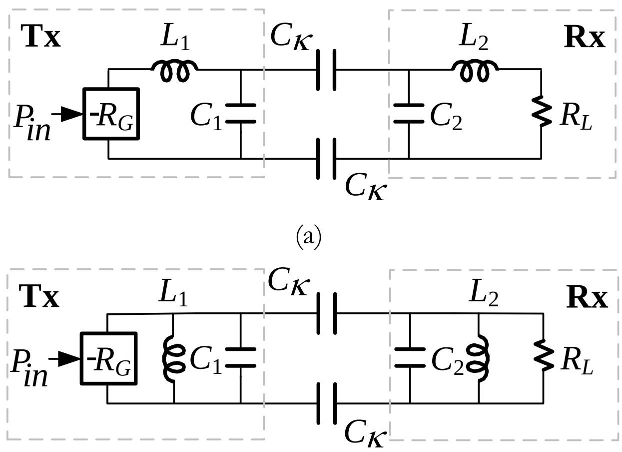

(b)

Fig. 1. $\mathcal{PT}$-symmetric capacitively coupled resonant system (a) coupled Tx-Rx series resonators, (b) coupled Tx-Rx parallel resonators.

Similar to other systems with the $\mathcal{PT}$-symmetry, the characteristic of the $\mathcal{PT}$-CPT exhibits two distinct operating phases depending on the relative magnitudes of the gain/loss element and the capacitive coupling. During the so-called *exact* phase, the power from the gain element of the Tx resonator perfectly counterbalances the dissipation in the Rx resonator. This, as a consequence, gives rise to even energy distribution between the two resonators, and therefore purely real eigen-frequencies with sustained oscillation amplitudes are obtained. On the contrary, during the *broken* phase, the energy in the two resonators is unbalanced, yielding complex eigen-frequencies, with exponentially growing and decaying oscillations.

By applying the Kirchhoff's voltage and current laws on the series and parallel $\mathcal{PT}$-CPT circuits of Fig. 1(a) and 1(b), it can be shown that the governing equations in terms of the capacitance charges $Q_{1,2} = C_{1,2}V_{C1,2} = CV_{C1,2}$ are given by

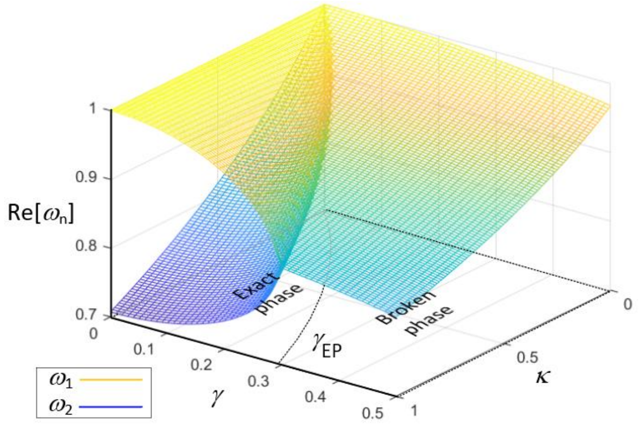

(a)

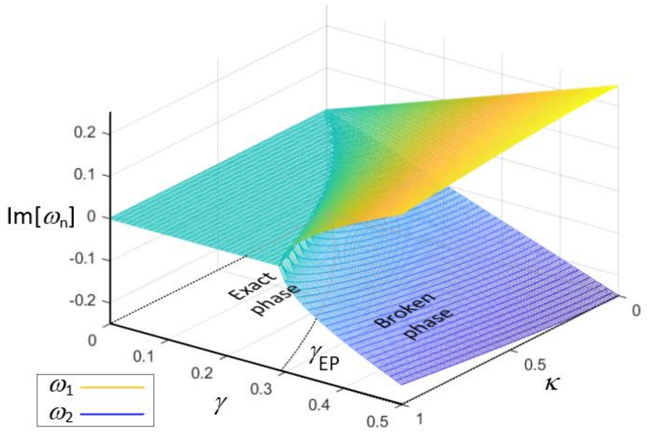

(b)

Fig. 2. Eigen-frequency characteristics versus non-Hermiticity parameter γ and coupling factor κ in $\mathcal{PT}$-CPT using series resonators. (a) real part, (b) imaginary part with exact and broken phase boundary.

$$\frac{d^2Q_1}{d\tau^2} = -\frac{\kappa+1}{2\kappa+1}Q_1 - \frac{\kappa}{2\kappa+1}Q_1 + \gamma\left(\alpha\kappa + \frac{\kappa+1}{2\kappa+1}\right)\frac{dQ_1}{d\tau} - \gamma\left(\alpha\kappa + \frac{\kappa}{2\kappa+1}\right)\frac{dQ_1}{d\tau} \quad (1a)$$

$$\frac{d^2Q_2}{d\tau^2} = -\frac{\kappa}{2\kappa+1}Q_2 - \frac{\kappa+1}{2\kappa+1}Q_2 + \gamma\left(\alpha\kappa + \frac{\kappa}{2\kappa+1}\right)\frac{dQ_2}{d\tau} - \gamma\left(\alpha\kappa + \frac{\kappa+1}{2\kappa+1}\right)\frac{dQ_2}{d\tau} \quad (1b)$$

where $\kappa = C_\kappa/C$ is the capacitive coupling factor and γ is the gain/loss or non-Hermiticity parameter. For the series configuration of Fig. 1(a), we have $\alpha = 1$ and $\gamma = R/\sqrt{L/C}$, and for the parallel configuration, $\alpha = 0$ and $\gamma = R^{-1}\sqrt{L/C}$. Also, $\tau = \omega_0 t$, or the frequency unit in these equations is normalized by the resonance frequency ω_0. As evident from (1), the equations remain unchanged via the combination of the parity $\mathcal{P}$ ($Q_1 \leftrightarrow Q_2$) and time-reversal $\mathcal{T}$ ($t \leftrightarrow -t$) transformations.

Equation (1) can be written in form of a rate-equation through Liouvillian's formalism [12] as

$$\frac{d\Psi}{d\tau} = \mathcal{L}\Psi;$$

$$\mathcal{L} = \begin{pmatrix} 0 & 0 & 1 & 0 \\ 0 & 0 & 0 & 1 \\ -\frac{\kappa+1}{2\kappa+1} & -\frac{\kappa}{2\kappa+1} & \gamma\left(\alpha\kappa+\frac{\kappa+1}{2\kappa+1}\right) & -\gamma\left(\alpha\kappa+\frac{\kappa}{2\kappa+1}\right) \\ -\frac{\kappa}{2\kappa+1} & -\frac{\kappa+1}{2\kappa+1} & \gamma\left(\alpha\kappa+\frac{\kappa}{2\kappa+1}\right) & -\gamma\left(\alpha\kappa+\frac{\kappa+1}{2\kappa+1}\right) \end{pmatrix} \quad (2)$$

where $\Psi = [Q_1, Q_2, dQ_1/d\tau, dQ_2/d\tau]^T$. Subsequently, by putting $Q_{1,2} = A_{1,2}e^{i\omega\tau}$, i.e., in form of time-harmonic function and solving the eigen-value equations associated with (2), the eigen-frequencies as function of the gain/loss parameter γ and the coupling factor κ can be derived as

$$\omega_{1,3} = \pm\sqrt{\frac{\alpha - f\big((\gamma^2-1),(\kappa+1)\big) + \sqrt{[f((\gamma-1)^2,(\kappa+1)) - \alpha]\cdot[f((\gamma+1)^2,(\kappa+1)) - \alpha]}}{2(\kappa+1)}}$$

$$\omega_{2,4} = \pm\sqrt{\frac{\alpha - f\big((\gamma^2-1),(\kappa+1)\big) - \sqrt{[f((\gamma-1)^2,(\kappa+1)) - \alpha]\cdot[f((\gamma+1)^2,(\kappa+1)) - \alpha]}}{2(\kappa+1)}} \quad (3)$$

where $f(x,y) = x\cdot y$ for the series configuration, $f(x,y) = x - y$ for the parallel configuration, with α and γ as defined previously.

Let us now examine the characteristic of the eigen-frequencies versus γ and κ. Note that the series and parallel configurations exhibit similar characteristics, and only a series $\mathcal{PT}$-CPT employed in the demonstrated wireless power transfer system of the next section is considered. Based on (3) with $f(x,y) = x\cdot y$, $\alpha = 1$ and $\gamma = R/\sqrt{L/C}$, the evolutions of the real and imaginary parts of the normalized eigen-frequencies versus $\gamma \in [0, 0.5]$ and $\kappa \in [0, 1.0]$ are shown in Fig. 2(a) and 2(b), respectively. To simplify the plots, only the two distinct positive frequencies ω_1 ($=-\omega_3$) and ω_2 ($=-\omega_4$) in (3) are given.

At $\gamma = 0$, or equivalently no loss and gain ($R = 0$) for a series configuration, the two eigen-frequency pairs are $\omega_{1,3} = \pm 1$ and $\omega_{2,4} = \pm 1/\sqrt{\kappa+1}$. When the resonators are isolated, i.e., at zero capacitive coupling $\kappa = 0$, this results in double degenerated frequencies $\omega_1 = \omega_2 = +1$ (and $\omega_3 = \omega_4 = -1$) with units of ω_0. In the exact phase region of Fig. 2(a), the CPT system exhibits two distinct and purely real eigen-frequency pairs, with associated sustained oscillatory responses. The purely real eigen-frequencies ω_1 and ω_2 (also ω_3 and ω_4) coalesce at the exceptional point γ_{EP}, which is a function of the coupling κ and can be derived from (3) as

DOI:10.4186/ej.2022.26.6.73

$$\gamma_{EP} = \frac{\sqrt{\kappa+1}-1}{(\kappa+1)^{\alpha/2}} \quad (4).$$

The plot of γ_{EP} versus κ boundary line using (4) at $\alpha = 1$ for a series configuration is also included in Fig. 2(a) and 2(b). Subsequently in the broken phase region, the eigen-frequencies bifurcate and branch out to complex values as shown in Fig. 2(b), yielding associated exponential growing and damping oscillations. The described characteristic is essentially similar to the $\mathcal{PT}$-symmetric IPT [13, 14]. This strongly indicates that the same power transfer robustness over extended distances can be harnessed in the $\mathcal{PT}$-symmetric CPT system.

3. Practical Application and Simulation

To verify the analysis and demonstrate the practical feasibility, a nonlinear $\mathcal{PT}$-CPT system was designed and simulated. It features significant improvement over the conventional CPT by offering robust power transfer and high efficiency, while maintaining all the advantages of the capacitive coupling system. The nonlinear $\mathcal{PT}$-CPT is the dual system of its $\mathcal{PT}$-IPT counterpart in [14] with the incorporation of the nonlinear gain element in the Tx resonator with its operating frequency automatically adjusted for optimum power transfer without external tuning. One of the target applications of this design is to serve as a through-wall/mirror wireless powering or charging of outdoor electronic devices. An example includes a fixed wireless access for millimetre-wave 5G networks, which have to be installed outside a premise to avoid very low signal penetration at such frequencies.

Figure 3 illustrates the schematic of the nonlinear $\mathcal{PT}$-CPT circuit with a series configuration for both the gain and loss sides of the coupled Tx-Rx resonators. The circuit was designed to deliver more than 10-Watts of power from the Tx resonator to a 20-Ohm load R_L on the Rx resonator with a high efficiency over a 20-cm separating or transfer distance *d*. It makes use of the four-plate structure for C_κ's, each with the dimension of 30.0 cm x 60.0 cm. Based on an electromagnetic (EM) simulation, this yielded the coupling capacitance C_κ in the range of 179.8pF to 11.4pF over the distance *d* from 1-cm to 100-cm. The nominal resonance frequency of the resonators at zero coupling $\kappa = 0$ was set at 2.37 MHz, similar to its nonlinear $\mathcal{PT}$-IPT counterpart in [14]. With the selected capacitance $C =$ 250pF to obtain a coupling factor between $\kappa =$ 0.046 to 0.720 over the distance d, the inductance values $L_1 = L_2 = 18\ \mu$H were determined at the nominal resonance frequency. The nonlinear gain element (inside the dash box of Fig. 3) was based on a positive-feedback class-E switching amplifier [15, 16] using a Gallium Nitride transistor, GS61008T (with the simulation model provided in [17]). For a 10-W load power at R_L, the GAN transistor run on a 15.0-V supply voltage V_{dd} with a 100 μH radio-frequency choke. The drain capacitance was calculated at

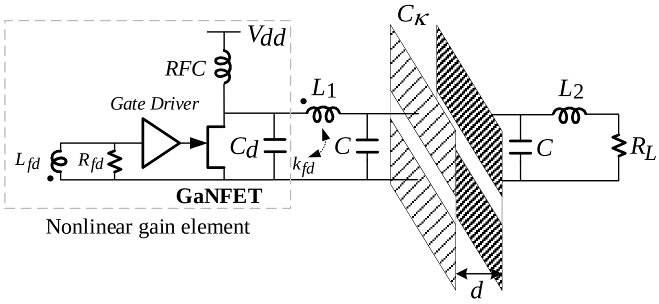

Fig. 3 Practical nonlinear $\mathcal{PT}$-CPT schematic using positive-feedback class-E switching power amplifier and four-plate coupling structure.

$C_d \approx$ 500pF for optimal class-E switching condition. The feedback path was set up via the coupled series inductors L_1 to L_{fd} with a mutual coupling factor $k_{fd} = 0.01$. The variable parallel resistor R_{fd} was included for fine phase adjustment of the feedback signal. The gate driver was a combination of an LT1711 comparator and an LM5114 driver with a 5-V supply. Note that circuit simulation was performed using LTspice [18].

Figure 4(a) shows the variation of the simulated oscillation frequency versus transfer distance d of the $\mathcal{PT}$-CPT circuit. Also included for comparison is the underlying theoretical eigen-frequencies (in MHz unit) with the branching characteristic, based on (3) and the described circuit parameters. In the exact phase, only the oscillation frequency associated with the high eigen-frequency value is sustained. This is attributed to the fact that, for the capacitive coupling system, the high eigen-frequency oscillation requires the lowest loop gain to reach its steady state, thereby saturating the amplifier and preventing the low eigen-frequency mode to grow further. This is contrast to the nonlinear $\mathcal{PT}$-IPT, where the low eigen-frequency mode is maintained since this requires the lowest loop gain in the inductive coupling system [14]. Overall, it is seen from the plot of Fig. 4(a) that the simulated oscillation frequencies versus the distance *d* are in close agreement with the theoretically calculated high eigen-frequency mode throughout the exact and broken operating phases.

The plots of the simulated power transfer level and efficiency versus the transfer distance d are shown in Fig. 4(b). As evident, the transferred power of the nonlinear $\mathcal{PT}$-CPT system is well maintained in the exact phase and only gradually decreased in the broken phase beyond the distance $d =$ 6-cm where the theoretical eigen-frequencies coalesce, i.e., at the exceptional point, in Fig. 4(a). Specifically, it can deliver a power level more than 10.0 Watts and a high efficiency at about 90% over the distance more than 20-cm. Also included in the plots are the comparative performances of the conventional CPT, where the feedback components L_{fd} and R_{fd} in the circuit of Fig. 3 were replaced by a 2.37-MHz frequency Tx source driving the gate driver. Clearly from Fig. 4(b),

DOI:10.4186/ej.2022.26.6.73

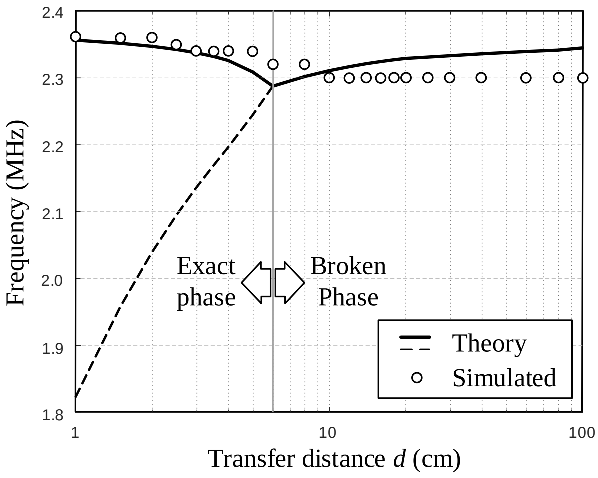

(a)

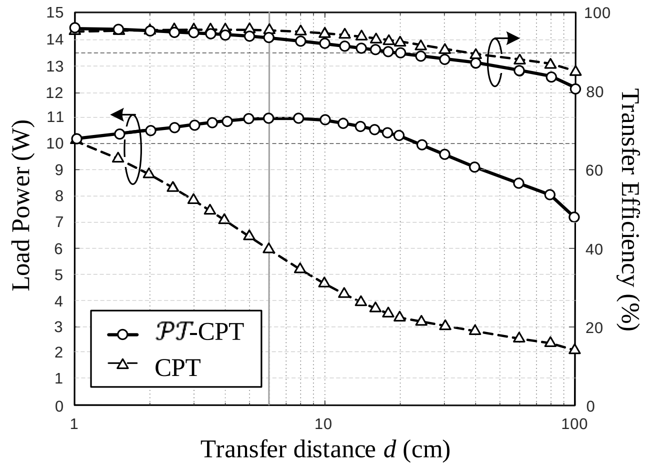

(b)

Fig. 4. Demonstrated nonlinear $\mathcal{PT}$-CPT system. (a) simulated and theoretical eigen-frequencies versus distance (b) simulated load power and efficiency versus distance in comparison with conventional CPT.

the power transfer level of the conventional CPT sharply drops with the distance d. Compared to the transfer distance at d > 20-cm in the non-linear $\mathcal{PT}$-CPT, the conventional CPT only deliver 10.0 Watts of power up to $d = 1$-cm. This indicates an improvement by more than twenty folds with no requirement of complex automatic tuning circuitry. It is noted that slightly less efficiency is observed in the $\mathcal{PT}$-CPT, and this is simply due to its higher power operating level, and hence a larger duty cycle and a higher switching loss in the class-E power amplifier.

4. Conclusion

A parity-time symmetric capacitive wireless power system has been developed to solve the performance bottleneck due to inherently low capacitive couplings. Its characteristic has been analytically derived, and practical feasibility has been verified via simulation. By virtue of automatic adjustment of the optimum operation at the lowest gain eigen-frequency mode, the nonlinear $\mathcal{PT}$-CPT using a positive-feedback switching-mode amplifier for the gain element has been demonstrated to offer considerable extension of the power transfer distance with high efficiency. Such effectiveness with low complexity has outperformed other compensation techniques for distance extension in the conventional CPT [10], [19, 20].

The parity-time symmetric CPT should find itself complementary to currently more ubiquitous inductive counterpart. In particular, it holds promise to more successful deployment of the CPT in applications hostile to the IPT system, such as those with metal surroundings or light weight requirement. This, together with simple and inexpensive implementation of capacitive coupling plates could pave the way for more pervasive utilization of wireless power delivery in electronic systems. Experimental implementation of the PT-CPT system with measurement will be reported in our future work.

References

[1] S. Y. R. Hui, W. Zhong, and C. K. Lee, "A critical review of recent progress in mid-range wireless power transfer," *IEEE Trans. Power Electron.*, vol. 29, no. 9, pp. 4500–4511, 2014.

[2] X. Lu, P. Wang, P., D. Niyato, D. I. Kim, and Z. Han, "Wireless charging technologies: Fundamentals, standards, and network applications," *IEEE Commun. Surv. Tutor.*, vol. 18, pp. 1413–1452, 2016.

[3] C. C. Mi, G. Buja, S. Y. Choi, and C. T. Rim, "Modern advances in 1150 wireless power transfer systems for roadway powered electric vehicles," *IEEE Trans. Ind. Electron.*, vol. 63, no. 10, pp. 6533–6545, 2016.

[4] P. K. Chittoor, B. Chokkalingam, and L. Mihet-Popa, "A review on UAV wireless charging: Fundamentals, applications, charging techniques and standards," *IEEE Access*, vol. 9, no. 4, pp. 69235–69266, 2021.

[5] Z. Cheng, Y. Lei, K. Song, and C. Zhu, "Design and loss analysis of loosely coupled transformer for an underwater high-power inductive power transfer system," *IEEE Trans. Magn.*, vol. 51, no. 7, pp. 1–10, 2015.

[6] S. Li, Z. Liu, H. Zhao, L. Zhu, C. Shuai, and Z. Chen, "Wireless power transfer by electric field resonance and its application in dynamic charging," *IEEE Trans. Ind. Electron.*, vol. 63, pp. 6602–6612, 2016.

[7] M. Tamura, Y. Naka, K. Murai, and T. Nakata, "Design of a capacitive wireless power transfer system for operation in fresh water," *IEEE Trans. Microw. Theory Tech.*, vol. 66, pp. 5873–5884, 2018.

[8] H. Zhang, F. Lu, and C. Mi, "An electric roadway system leveraging dynamic capacitive wireless charging: Furthering the continuous charging of

electric vehicles," *IEEE Trans. Electrif. Mag.*, vol. 8, pp. 52–60, 2020.

[9] J. Dai and D. C. Ludois, "A survey of wireless power transfer and a critical comparison of inductive and capacitive coupling for small gap applications," *IEEE Trans. Power Electron.*, vol. 30, pp. 6017–6029, 2015.

[10] C. Lecluyse, B. Minnaert, and M. Kleeman, "A review of the current state of technology of capacitive power transfer," *Energies.*, vol. 14, pp. 5862–5884, 2021.

[11] C. M. Bender, and S. Boettcher, "Real spectra in non-Hermitian Hamiltonians having PT symmetry," *Phys. Rev. Lett.*, vol. 80, no. 24, pp. 5243–5248, 1998.

[12] J. Schindler, A. Li, M. C. Zheng, F. M. Ellis, and T. Kottos, "Experimental study of active LRC circuits with PT symmetries," *Phys. Rev. A*, vol. 84, no. 4, 2011.

[13] S. Assawaworrarit, X. Yu, and S. Fan, "Robust wireless power transfer using a nonlinear parity-time symmetric circuit," *Nature*, vol. 546, pp. 387–390, 2017.

[14] S. Assawaworrarit and S. Fan, "Robust and efficient wireless power transfer using a switched-mode implementation of a nonlinear parity-time symmetric circuit," *Nat. Electron.*, vol. 3, pp. 273–279, 2020.

[15] N. O. Sokal, and A. D. Sokal, "Class E, a new class of high-efficiency tuned single-ended power amplifiers," *IEEE Journal of Solid-State Circuits*, vol. 10, pp. 168-176, June 1975.

[16] T. H. Lee, *Design of CMOS Radio-Frequency Integrated Circuits*, 2nd ed. Cambridge, UK: Cambridge University Press, 2004.

[17] *GAN Systems: 'Spice model of GS61008T'.* https://gansystems.com/gan-transistors/gs61008t/, (accessed December 2021).

[18] *Analog Devices: 'LTspice®: SPICE circuit simulation software', version 17.0.32.0.* https://www.analog.com/en/design-center/design-tools-and-calculators/ltspice-simulator.html, (accessed December 2021).

[19] M. P. Theodoridis, "Effective capacitive power transfer," *IEEE Trans. Power Electron.*, vol. 27, no. 12, pp. 4096 – 4913, 2012.

[20] S. Sinha, A. Kumar, B. Regensburger, and K. K. Afridi, "Design of high frequency matching network for capacitive wireless power transfer," *IEEE Journal Emerg. Sel. Top. Power Electron.*, vol. 10, no. 1, pp. 104 – 127, 2022.

Panavy Pookaiyaudom received his bachelor degree in Electronic Systems Design from Oxford Brookes University in 2006 and completed his PhD in Electrical Engineering (Analogue Integrated Circuit Design) from Imperial College London, in 2011.

Since 2011, he has joined Department of Electronics Engineering at Mahanakorn University of Technology and also appointed the director of Centre for Bioelectronics Integrated System and Applied Innovation. His research interests include fully integrated bio-chemical sensors, biomedical and bio-inspired technology, low power analogue signal processing, semiconductor platforms for DNA and robotics technology

Apisak Worapishet received the B.Eng. (Hons.) degree from the King Mongkut's Institute of Technology Ladkrabang, Bangkok, Thailand, in 1990, the M.Eng.Sc. degree from the University of New South Wales, Kensington, NSW, Australia, in 1995, and the Ph.D. degree from the Imperial College London, London, U.K., in 2000, all in electrical engineering.

Since 1990, he has been with the Mahanakorn University of Technology, Bangkok, Thailand, where he is currently a Professor of electronic engineering. He is also the director of the Mahanakorn Microelectronics Research Center and a Lecturer with the Mahanakorn Institute of Innovation, Bangkok, Thailand. His research interests include analogue integrated circuits, passive/active RF/microwave circuits, and wireless power transfer.

Dr. Worapishet has been an Associate Editor for the IEEE TRANSACTIONS ON CIRCUITS AND SYSTEMS I: REGULAR PAPERS since 2016. He was the Editor-in-Chief for ECTI Transactions on Electrical Engineering, Electronics, and Communications from 2012 to 2019. He is an IEEE Senior member, a member of the Analog Signal Processing Technical Committee and the IEEE Circuits and Systems Society. He was the recipient of the British Council Researcher Exchange Program Award in 2009.